HHS Public Access

Author manuscript

Phys Med Biol. Author manuscript; available in PMC 2016 May 07.

Published in final edited form as:

Phys Med Biol. 2015 May 7; 60(9): 3731–3746. doi:10.1088/0031-9155/60/9/3731.

Imaging and dosimetric errors in 4D PET/CT-guided radiotherapy from patient-specific respiratory patterns: a dynamic motion phantom end-to-end study

S R Bowen[1,2], **M J Nyflot**[1], **C Hermann**[3], **C Groh**[4], **J Meyer**[1], **S D Wollenweber**[5], **C W Stearns**[5], **P E Kinahan**[2], and **G A Sandison**[1]

[1]Department of Radiation Oncology, University of Washington School of Medicine, Seattle, WA, USA

[2]Department of Radiology, University of Washington School of Medicine, Seattle, WA, USA

[3]Department of Computer Science, University of Würzburg, Würzburg, Germany

[4]Department of Radiation Oncology, University Hospital of Würzburg, Würzburg, Germany

[5]GE Healthcare Systems, Waukesha, WI, USA

Abstract

Effective positron emission tomography/computed tomography (PET/CT) guidance in radiotherapy of lung cancer requires estimation and mitigation of errors due to respiratory motion. An end-to-end workflow was developed to measure patient-specific motion-induced uncertainties in imaging, treatment planning, and radiation delivery with respiratory motion phantoms and dosimeters. A custom torso phantom with inserts mimicking normal lung tissue and lung lesion was filled with [^{18}F]FDG. The lung lesion insert was driven by 6 different patient-specific respiratory patterns or kept stationary. PET/CT images were acquired under motionless ground truth, tidal breathing motion-averaged (3D), and respiratory phase-correlated (4D) conditions. Target volumes were estimated by standardized uptake value (SUV) thresholds that accurately defined the ground-truth lesion volume. Non-uniform dose-painting plans using volumetrically modulated arc therapy (VMAT) were optimized for fixed normal lung and spinal cord objectives and variable PET-based target objectives. Resulting plans were delivered to a cylindrical diode array at rest, in motion on a platform driven by the same respiratory patterns (3D), or motion-compensated by a robotic couch with an infrared camera tracking system (4D). Errors were estimated relative to the static ground truth condition for mean target-to-background (T/B_{mean}) ratios, target volumes, planned equivalent uniform target doses (EUD), and 2%-2mm gamma delivery passing rates. Relative to motionless ground truth conditions, PET/CT imaging errors were on the order of 10–20%, treatment planning errors were 5–10%, and treatment delivery errors were 5–30% without motion compensation. Errors from residual motion following compensation methods were reduced to 5–10% in PET/CT imaging, < 5% in treatment planning, and < 2% in treatment delivery. We have demonstrated that estimation of respiratory motion uncertainty and its propagation from PET/CT imaging to RT planning, and RT delivery under a

Corresponding author contact information: Stephen R. Bowen, Ph.D., 1959 N.E. Pacific St. Box 356043, Seattle, WA 98195, Office: (206) 598-1128, Fax: (206) 598-6218, srbowen@uw.edu.

dose painting paradigm is feasible within an integrated respiratory motion phantom workflow. For a limited set of cases, the magnitude of errors was comparable during PET/CT imaging and treatment delivery without motion compensation. Errors were moderately mitigated during PET/CT imaging and significantly mitigated during RT delivery with motion compensation. This dynamic motion phantom end-to-end workflow provides a method for quality assurance of 4D PET/CT-guided radiotherapy, including evaluation of respiratory motion compensation methods during imaging and treatment delivery.

Keywords

PET/CT; respiratory motion; IGRT; VMAT; dose painting; robotic couch tracking

1. Introduction

Positron emission tomography (PET) and computed tomography (CT) multimodality imaging has exhibited high diagnostic (Weber *et al.*, 2008; Juweid and Cheson, 2006) and prognostic value (Vansteenkiste *et al.*, 1998; Imamura *et al.*, 2011) in the detection and staging of cancer patients. However, the quantitative application of PET/CT for defining therapeutic targets (Caldwell *et al.*, 2001; Senan and De Ruysscher, 2005; Bettinardi *et al.*, 2010b) and assessing therapeutic response (Avril and Weber, 2005) remains a challenge in clinical practice. Specifically in radiation oncology, the integration of PET/CT into radiation therapy planning and delivery is complex and burdened by uncertainties that are technical, physical, and biological in nature (Boellaard, 2009; Mac Manus *et al.*, 2003; Nestle *et al.*, 2006). From uncertainties in the PET-based segmentation of target volumes (Nestle *et al.*, 2005; Cheebsumon *et al.*, 2012) to generation of optimized and deliverable PET-based radiotherapy dose distributions (Bowen *et al.*, 2009), the magnitude of error varies widely between patients and even within individuals.

Phantom studies provide estimates on the magnitude of these uncertainties relative to representative ground truth images, radiotherapy plans, and delivery measurements, which is otherwise unavailable in patient data. This also helps to identify the major source of uncertainty and direct resources to reinforce the workflow chain at its weakest link. Some researchers have superimposed realistic tracer uptake distributions onto virtual anthropomorphic phantoms that enable the simulation of PET images to validate target definition methods for radiotherapy planning, while others have calibrated physical phantoms with variable lesion characteristics to compare directly to ground truth measurement conditions (Ford *et al.*, 2006; Ford *et al.*, 2009; Tylski *et al.*, 2010). Similarly, the assessment of intensity-modulated radiotherapy (IMRT) and volumetrically modulated arc therapy (VMAT) delivery accuracy has been conducted by comparing the measured dose and planned dose in a standard phantom geometry, each generated from the same patient planned radiation fluence map (Low and Dempsey, 2003; Ezzell *et al.*, 2003).

In certain disease sites, such as lung cancer, a major source of uncertainty for PET/CT-guided radiotherapy is respiratory-induced tumour and normal-tissue motion, which can impact both imaging and treatment delivery to degrees that are patient and technology-dependent (Nehmeh *et al.*, 2004; De Ruysscher *et al.*, 2012; Liu *et al.*, 2009; Kissick *et al.*,

2010). Improved quantification in the presence of respiratory motion with motion-compensated (4D) PET/CT (Bettinardi *et al.*, 2010a) has potential synergies with motion-compensated (4D) radiotherapy (Li *et al.*, 2008) to administer biologically conformal lung cancer treatments that would enable non-uniform tumour dose escalation. These synergies are clinically motivated by the correlation between high 2-deoxy-2-[^{18}F]fluoro-D-glucose ([^{18}F]FDG) PET uptake and poor overall survival in advanced non-small cell lung cancer patient populations (van Elmpt *et al.*, 2012), as well as co-localization of avid FDG PET regions and local residual disease post treatment (Aerts *et al.*, 2012).

Methods for managing uncertainty due to motion through proposed 4D PET/CT-guided radiotherapy (Aristophanous *et al.*, 2012; Aristophanous *et al.*, 2011; Bettinardi *et al.*, 2012) have revealed little consensus on which combined motion-compensated imaging and treatment delivery method is best suited to an individual patient (Bowen *et al.*, 2012; Keall *et al.*, 2006). Investigations on motion-induced errors in PET/CT have estimated differences in SUV_{max} between 3D and 4D PET/CT on the order of 7–12% in patients with phase gating and amplitude gating methods, while differences in tumour volume between 3D and 4D PET/CT were highly variable due to segmentation technique (Nehmeh *et al.*, 2004; van Elmpt *et al.*, 2011). Investigations on motion-induced errors in radiotherapy have estimated differences in mean delivered IMRT target dose for a single fraction on the order of 30% for individual fields but reduced to under 5% when averaging over all fields and treatment fractions (Bortfeld *et al.*, 2004; Webb, 2006a, b; Duan *et al.*, 2006). Fixed or adaptive beam gating (Berbeco *et al.*, 2005; Li *et al.*, 2008; Aristophanous *et al.*, 2010), dynamic MLC tracking (Webb, 2006b; Falk *et al.*, 2012; Keall *et al.*, 2014), and robotic couch tracking (Menten *et al.*, 2012) can reduce these dosimetric errors in a single fraction to within 2% (Flampouri *et al.*, 2006; Wilbert *et al.*, 2013), but these and other studies focused exclusively on CT-based targets receiving uniform dose. The magnitude of these effects is more pronounced for high dose rate, hypofractionated VMAT delivery of non-uniform dose distributions with steep spatial gradients (Court *et al.*, 2010), which requires carefully generated treatment margins (Shah *et al.*, 2013).

To date, the estimation of respiratory motion-induced errors in aggregate from all steps in 4D PET/CT-guided radiotherapy workflows has neither been proposed nor reported on due in part to limited understanding of how these errors propagate from imaging to planning to treatment delivery. The purpose of this study is to design an integrated end-to-end 4D PET/CT-guided radiotherapy workflow in dynamic phantoms that evaluates and propagates motion-induced errors relative to motionless ground truth conditions. The approach may provide clinical utility as a quality assurance tool for FDG PET-based dose painting in patients with mobile lung tumours. We report errors in a select few approaches of the workflow, shown schematically in Figure 1 and listed below:

1. Motionless (ground truth): PET/CT, radiotherapy plan, and radiotherapy delivery under no motion
2. Tidal breathing (clinical): PET/CT ungated under motion, radiotherapy plan based on motion-averaged PET/CT, and radiotherapy delivery under motion

3. Respiratory-correlated (4D): PET/CT phase-gated under motion, radiotherapy plan on end-exhale phase, and radiotherapy delivery under motion with robotic couch tracking

2. Materials and methods

2.1 Dynamic motion phantoms

To characterize motion-induced errors in a 4D PET/CT-guided workflow, imaging and radiotherapy motion phantoms were utilized. The imaging phantom consisted of a Quasar Multipurpose Body Phantom™ (Modus Medical, Inc.), a custom PET/CT lung insert, and a Quasar Respiratory Motion Assembly™ (Modus Medical, Inc.). The lung insert was machined in-house to contain a single fillable spherical lesion surrounded by polystyrene beads that mimicked lung tissue-equivalent density corresponding to −700 HU on CT (nominal). The lung background was filled independently from the lesion to vary image contrast. The motion assembly drove the lung insert with patient-specific respiratory patterns in the superior-inferior axis. The lung insert was mechanically coupled to a platform that enables prospective respiratory-gated or retrospective respiratory-correlated (4D) PET/CT acquisitions through use of the Real-time Position Management™ (RPM, Varian, Inc.) system, which consists of infrared camera tracking of a marker block placed on the patient chest/abdomen. Details of the PET/CT and RPM system can be found in prior investigations (Liu *et al.*, 2010).

The radiotherapy phantom comprised an ArcCHECK™ (Sun Nuclear, Inc.) cylindrical diode detector array and a Quasar Motion Platform™ (Modus Medical, Inc.). The platform drove the diode array with the same patient-specific respiratory patterns as the imaging phantom, which allowed for a complete propagation of motion-induced errors along the 4D PET/CT-guided radiotherapy workflow. Both dynamic motion phantoms are shown in Figure 2 (top row) with the same patient respiratory pattern displayed.

2.2 PET/CT imaging

A spherical phantom insert of 2.2 cm diameter was chosen to represent a typical lung lesion. The spherical insert and lung-equivalent density insert were filled with a fixed target-to-background contrast ratio (10:1 nominal) of [^{18}F]FDG to mitigate the influence of image noise on motion-induced uncertainties. The phantom was scanned in 3D mode on a Discovery STE™ PET/CT scanner (GE Healthcare) (Teras *et al.*, 2007) at a single 15 cm axial field-of-view for a 5 min static acquisition without motion, a 5 min static acquisition with motion, and a 5 min x 5 bin respiratory phase-gated acquisition with motion. Acquisitions resulted in 5 million total counts and lesion activity concentrations of 0.05 MBq/mL (nominal). The ground truth image without motion was attenuation-corrected with a helical CT, the motion-blurred image was corrected with a phase-averaged cine CT, and the motion-compensated images were corrected with a phase-matched cine CT (Killoran *et al.*, 2011). 4D phase-matched PET/CT were processed on the GE DSTE scanner and/or GE 4D Advantage workstation. All PET images were corrected for scatter, randoms, and normalization but did not include resolution modelling or partial volume corrections. Images were reconstructed with ordered subset expectation-maximization (OSEM) over 2 iterations and 28 subsets, filtered with a 5 mm wide Gaussian post-reconstruction filter, and sampled

onto a 50 cm transverse field-of-view grid of 1.95 mm x 1.95 mm x 3.27 mm voxels. Example PET and CT images are shown in Figure 2 for motionless, motion-blurred under tidal breathing, and motion-compensated (end-exhale phase) conditions (left side).

2.3 Radiotherapy planning

PET/CT images were imported into the MIM™ v6.0 (MIM, Inc.) software for radiotherapy planning target definition. From the ground truth motionless PET image, a fixed SUV_{max} percentage threshold was determined that matched the volume relative to the known sphere size reported by the manufacturer. The fixed threshold was then propagated to the motion-blurred and the motion-compensated PET image at reference end-exhale phase. Different target definition methods can be tested and contrasted to this approach (see Discussion). Normal lung and spinal cord contours were also defined on all torso phantom CT images. Images and structure sets were exported to the Pinnacle^{3}™ v9.2 (Philips Medical) treatment planning system to generate independent plans from helical, phase-averaged, and phase-gated cine CT.

Volumetrically modulated arc therapy (VMAT) plans were optimized in Pinnacle SmartArc™ (Philips Medical) for the motionless (ground truth), tidal breathing motion (clinical), and motion-compensated (4D end-exhale phase) conditions on Elekta Synergy linear accelerators, illustrated in Figure 2. The 6 MV beam configuration was defined as two partial dynamic arcs with avoidance of entrance dose through the contralateral lung and collimator angle of 25 degrees to minimize interleaf leakage. Normal tissue objectives were fixed for static, motion-blurred, and motion-compensated plans: normal lung $V_{20Gy} < 20\%$, spinal cord $D_{max} < 45$ Gy, and spinal cord $V_{23Gy} < 10\%$. The FDG PET-based dose painting target was shaped by a minimum dose objective of 60 Gy (2 Gy/fx) with peaked spatial distribution coinciding with the high lesion uptake. VMAT optimization was conducted under a leaf motion constraint of 0.3 cm per degree and control point spacing of 4 degrees. Objective functions for all plans converged within 40 iterations from a stopping tolerance of 10^{-5} relative change. To assess differences in non-uniform target dose distributions between plans, generalized equivalent uniform doses were calculated with generalized parameter $a = -10$ to penalize cold spots (Choi and Deasy, 2002; Wu *et al.*, 2005).

2.4 Radiotherapy delivery

The ArcCHECK radiotherapy phantom was placed on the Quasar motion platform and aligned to the treatment machine isocentre. The ground truth plan was delivered without respiratory motion, the motion-averaged plan (clinical) was delivered under matched patient respiratory motion trajectories from imaging, and the motion-compensated plan based on a reference end-exhale phase was delivered under matched respiratory motion trajectories with robotic couch tracking and compensation enabled. The latter simulated the most dosimetrically challenging scenario when tracking the lesion to deliver non-uniform radiation dose based on the highest PET uptake contrast observed at end-exhale phase. Measured dose to the ArcCHECK diode array was compared to the planned dose in the cylindrical detector plane using the SNC Patient™ (Sun Nuclear, Inc.) software. The planned dose, measured dose, and dose difference spatial distributions are shown in Figure 2.

Volumetric dose comparison in the original PET/CT imaging phantom was achieved using the Planned Dose Perturbation™ algorithm of the 3DVH™ software (Sun Nuclear, Inc.). The algorithm converted the measured dose in the ArcCHECK detector plane to an equivalent volumetric dose on the PET/CT imaging phantom by calculating the differential beam attenuation through the heterogeneous planning geometry relative to the homogeneous measurement geometry. Secondary corrections to the dose output for VMAT multi-leaf collimator (MLC) shapes were applied using a physics model of the Elekta Synergy linear accelerators.

Respiratory motion-compensated delivery was achieved with a robotic couch (Elekta HexaPOD) and infrared camera (NDI Poloaris Spectra) surface marker tracking technique. Details of the Adaptive Tumour Tracking System at the University of Würzburg have been published previously (Wilbert *et al.*, 2008) and the setup is shown in Figure 3. The strength of the tracking algorithm resides in its fast sub-second training period, which enables high predictive accuracy during intra-patient variation in respiratory pattern while maintaining patient comfort (Herrmann and Schilling, 2013). Robotic couch tracking was shown to provide similar geometric accuracy to MLC tracking but superior dosimetric accuracy in a direct comparative study (Menten *et al.*, 2012).

2.5 Error analysis

Errors were defined in each step of the workflow for several quantitative parameters. The error in each parameter was tabulated under tidal breathing motion (clinical) or respiratory motion compensation (4D) conditions as the relative difference to the motionless ground truth condition. For example, the relative error in the target volume V due to motion and residual error due to motion compensation would be calculated as follows:

$$\sigma(V)_{\text{motion}} = \frac{V_{\text{motion}} - V_{\text{truth}}}{V_{\text{truth}}} \quad (1)$$

$$\sigma(V)_{\text{compensated}} = \frac{V_{\text{compensated}} - V_{\text{truth}}}{V_{\text{truth}}} \quad (2)$$

For PET/CT images, the target-to-background ratio was calculated from the maximum lesion activity concentration normalized to the ipsilateral lung background activity concentration $(T/B)_{max}$. Errors under motion-averaged acquisition and residual errors under motion-compensated acquisition at reference end-exhale phase were recorded. The fixed SUV_{max} threshold defined the spherical target volume reported by the manufacturer. For VMAT plans, the maximum and equivalent uniform doses to the target were determined. Errors in the motion-averaged plan and residual errors in the motion-compensated plan at reference end-exhale phase were estimated. For radiotherapy delivery, dose deviations of 2 % and 2 mm distance-to-agreement tolerance criteria for gamma passing rates were recorded as a measure of delivery accuracy, along with maximum target dose. Errors in motion-blurred delivery and residual errors in motion-compensated and couch-tracked delivery were calculated.

3. Results

The feasibility of the 4D PET/CT-guided RT workflow was tested on a set of 6 patient respiratory trajectories recorded by the Varian RPM system with minimum and maximum absolute 1D displacement of 1.5 cm but unique amplitudes, periods, displacement deviations, and velocity deviations. A summary of the respiratory patterns is shown in Table 1. The motion-induced errors over this group of patient respiratory patterns are summarized in Table 2. The patient respiratory pattern representing the median of population errors is reported on in greater detail for each step of the workflow (Table 1: pattern 1).

3.1 Motion-induced PET/CT imaging errors

Target-to-background ratios $(T/B)_{max}$ were 11.2 for the static PET image, 9.0 for the motion-averaged PET, and 10.3 for the respiratory-gated PET at end-exhale phase, which corresponded to 20% and 8% median decreases, respectively. For the 2.2 cm diameter spherical target, a 34% SUV_{max} threshold calibrated to the static PET/CT image yielded the true volume of 5.6 cm^3. The 34% SUV_{max} target volume was 6.7 cm^3 in the motion-blurred PET/CT image and 5.9 cm^3 in the respiratory-gated PET/CT image, which corresponded to 15% and 7% median increases, respectively.

3.2 Motion-induced radiotherapy planning errors

All plans achieved the normal tissue objectives, resulting in mean lung doses of 5.1–5.5 Gy and maximum spinal cord dose of 10.7–13.3 Gy, as well as the target objective of 60 Gy minimum dose. Dose volume histograms of target and total lung structures are shown in Figure 4 for the static plan, motion-averaged plan, and motion-compensated plan. The maximum achievable target dose was 75.6 Gy for the static plan, 67.7 Gy for the motion-encompassing plan, and 73.5 Gy for the motion-compensated plan, which corresponded to 10% and 3% median decreases, respectively. Generalized EUD in the target were 69.5 Gy for the static plan, 64.8 Gy for the motion-averaged plan, and 67.9 Gy for the motion-compensated plan, which corresponded to 7% and 2 % median decreases, respectively.

3.3 Motion-induced radiotherapy delivery errors

Dosimetric errors in delivery were first assessed in the ArcCHECK cylindrical detector plane. The 2%-2mm gamma criteria passing rates are summarized in Figure 5 for the 6 respiratory patterns with superior-inferior trajectories. Delivery of the reference static plan based on a PET and helical CT with no motion achieves a 100% gamma pass rate. Delivery of the motion-encompassing plan based on a PET and average cine CT under the matching 6 patient respiratory patterns from imaging resulted in motion-averaged plan gamma ranges from 71–95% (median 85%). Delivery of the respiratory-gated and phase-matched PET/CT plans at end expiration with the same respiratory patterns under robotic couch tracking improves the gamma ranges to 98–100% (median 100%).

The measured dose in the radiotherapy phantom was reconstructed on the original PET/CT imaging phantom geometry, and the difference between measured and planned dose distributions is shown in Figure 6. The 2%-2mm gamma passing rates in the PET-based targets were 100% for the reference static plan under motionless delivery, 41%–80%

(median 61%) for the motion-averaged plan using 6 respiratory patterns during delivery, and 87–100% (median 100%) for the motion-compensated plan under couch-tracked delivery. The measured mean dose to the total lung was not significantly different between delivery conditions, ranging from 4.9–5.3 Gy. Maximum measured spinal cord dose was 10.7–11.4 Gy. Delivered dose DVH are illustrated in Figure 7, whereby the median errors in the measured maximum dose to the target were < −1% for the reference static plan under motionless delivery, −4% for the motion-averaged plan under various respiratory patterns during delivery, and < −1% for the motion-compensated plan under couch-tracked delivery.

3.4 Motion-induced aggregate errors

Aggregate errors were calculated from imaging, radiotherapy planning, and radiotherapy delivery errors in maximum tumour-to-background uptake ratio, maximum planned dose, and maximum delivered dose, respectively, by assuming that individual components summed in quadrature without interaction. Alternatively, the aggregate errors were directly measured as a percentage of the prescribed radiotherapy dose, which accounts for interaction of error terms when propagating from imaging to therapy delivery. The calculated and measured aggregate errors are listed in Table 2. Of note is that summing individual error components in quadrature overestimated the measured aggregate error, which implies an interaction between errors during imaging and radiotherapy delivery that dampened their combined magnitude. This effect is analogous to setup error averaging during fractionated radiotherapy, where sampling of respiratory motion patterns during PET/CT imaging can occur on a similar timescale as radiotherapy delivery. However, the degree to which error dampening takes place is likely patient-specific and affected by the periodicity of the respiratory motion pattern.

4. Discussion

Integrating PET/CT imaging into radiotherapy is complex, particularly in disease sites with respiratory motion-induced uncertainties. However, such integration could improve the quantitative accuracy and precision necessary for future implementation of 4D PET/CT-guided radiotherapy by informing the selection of respiratory motion management techniques during imaging and treatment. A workflow to measure errors from patient-specific respiratory motion during PET/CT imaging, treatment planning, and radiotherapy delivery was established using dynamic motion phantoms and dosimeters. Preliminary errors relative to reference motionless conditions were tabulated for a group of 6 patient respiratory patterns, showing that PET/CT imaging errors in contrast and target volume were on the order of 10–20%, treatment planning errors in maximum and equivalent dose were 5–10%, and treatment delivery errors in maximum dose and accuracy were 5–30% without motion compensation. Errors from residual motion following compensation methods were reduced to 5–10% in PET/CT imaging, < 5% in treatment planning, and < 2% in treatment delivery. In aggregate, the error in maximum delivered dose to the target under motion was 10 Gy (17% of prescription) less than under motionless ground truth conditions, whereas with motion compensation this error decreased to < 2 Gy (< 4% of prescription). These results suggest that the highest reduction in motion-induced errors occurred during treatment delivery with couch tracking, while the lowest reduction occurred during PET/CT imaging

when using conventional phase gating. This highlights the limitations of phase-gated imaging and fixed target volume thresholds in the presence of aperiodic respiratory motion, which may be addressed with more robust motion compensation and target definition approaches.

The generalized methodology with dynamic motion phantoms enables the evaluation of respiratory motion impact on a wide range of PET/CT imaging, treatment planning, and treatment delivery parameters as part of patient-specific quality assurance testing. While the imaging, planning, and delivery geometry is not patient specific, its standardization ensures that the effects of patient-specific respiratory motion are studied in isolation from numerous other parameters affecting PET/CT imaging and radiotherapy planning. Simulating the effects of patient-specific respiratory patterns relative to motionless ground truth conditions can lead to personalized approaches. For instance, the efficacy of PET/CT motion compensation techniques, from data-driven gating (Schleyer *et al.*, 2011; Schleyer *et al.*, 2009) to abdominal surface tracking and internal-external correlation modelling (Nehmeh *et al.*, 2011), could be determined relative to motionless acquisition conditions for each patient respiratory pattern. This includes advanced methods for correlating internal imaged motion and external surrogate motion that offer improved accuracy (Liu *et al.*, 2011). PET segmentation methods, such as gradient-based and stochastic algorithms (Hatt *et al.*, 2009), could be tested in the presence of respiratory motion to seek trade-offs between absolute volumetric accuracy and robustness to individual patient respiratory pattern variability. Comparison of PET-based treatment plans, for example uniform integrated dose boosts versus non-uniform dose painting (Ling *et al.*, 2000; Bentzen, 2005), could yield differences in sensitivity to an individual respiratory pattern. Finally, radiotherapy delivery compensation techniques could be simulated in terms of quantitative accuracy and precision for each individual patient treatment plan. Most importantly, these patient-specific quality assurance tests can be conducted in aggregate to form confidence intervals, which would represent a novel approach to patient motion management in PET/CT imaging and radiotherapy planning.

Long-term applications of these methods revolve around the administration of PET/CT-guided and motion-compensated radiotherapy for lung cancer. Through rigorous characterization of motion-induced errors for each patient, one can select robust compensation methods for imaging, planning, and treatment delivery. Mitigation of these errors can subsequently permit increasingly accurate radiation targeting of biological regions at greatest risk of treatment resistance, as well as modelling of regional imaging-based treatment response in tumour and normal tissue. These correlation studies have been reported on in disease sites that are less susceptible to respiratory motion (Bowen *et al.*, 2012; Nyflot *et al.*, 2012; Bradshaw *et al.*, 2013), but have the potential to be translated to lung cancer. Furthermore, determination of motion-induced errors for different radiotherapy modalities, such as proton and heavy-ion therapy, could inform on their clinical suitability for different patient cases.

Several limitations of the current study should be noted. Errors due to motion and residual errors due to motion compensation were estimated for a small number of cases and approaches, which does not fully sample the numerous potential approaches to 4D PET/CT-

guided radiotherapy (Figure 1). The observations and trends reported by this investigation may vary when different approaches are applied to patient imaging data with no ground truth and other sources of error (e.g. FDG tracer kinetics, anatomic variation). However, large magnitude errors characterized by this dynamic motion phantom workflow are useful to rule out approaches for clinical translation.

The robotic couch tracking of respiratory motion was limited by the use of independent but similar HexaPOD tables to produce and compensate for the motion, respectively. As the HexaPOD tables have upper bounds on velocity and acceleration, sharp inhale peaks that exceeded these bounds could not be fully reproduced. However, dosimetric measurements with both the Quasar motion platform and HexaPOD revealed that the largest deviation in error estimation were typically below 5%. This is likely due to the short time duration of the lesion at these sharp inhale peak positions relative to the total radiotherapy delivery time. Such a source of residual error that cannot be mitigated by robotic couch tracking could be incorporated as a spatial and/or dosimetric margin in the treatment plans.

The study also did not explicitly address the motion-induced errors from variable correlation between internal tumour motion and external marker, which impacts both motion-compensated imaging and treatment delivery. These are areas of future investigation, which would include the use of 3D respiratory motion trajectories, on-board imaging during delivery, and evaluation of tumour deformation errors secondary to rigid body motion.

5. Conclusion

An integrative end-to-end approach to estimate respiratory-motion induced uncertainties in PET/CT-guided radiotherapy of lung cancer is feasible. Reduction of these errors varied considerably between conventional phase-gated imaging and couch tracked radiotherapy delivery, with noticeable interaction between error components. Investigation of other motion management strategies is warranted to inform on future methods for dose painting of lung cancer, which may permit higher deliverable doses to motion-resolved biological targets at greatest risk of local disease recurrence. The workflow may be applied as both an evaluation tool of novel methods and a quality assurance tool in respiratory motion-compensated and PET/CT-guided radiotherapy of lung cancer, by simulating patient-specific conditions related to lesion size, lesion-to-background uptake and respiratory pattern for incorporation into target definition, treatment planning and delivery techniques.

Acknowledgments

This work was supported by NIH grant 5P30 CA015704, a research contract from GE Healthcare (Waukesha, WI), and a grant from the Bavarian Research Foundation (Germany). The authors are grateful to Dan Schindler for machining the PET/CT imaging phantom lung insert. Thanks to Lawrence MacDonald and Darrin Byrd for their assistance with the imaging phantom, as well as Julie Do for helping to acquire treatment delivery measurements with the radiotherapy phantom.

References

Aerts HJ, Bussink J, Oyen WJ, van Elmpt W, Folgering AM, Emans D, Velders M, Lambin P, De Ruysscher D. Identification of residual metabolic-active areas within NSCLC tumours using a pre-

radiotherapy FDG-PET-CT scan: a prospective validation. Lung Cancer. 2012; 75:73–6. [PubMed: 21782272]

Aristophanous M, Berbeco RI, Killoran JH, Yap JT, Sher DJ, Allen AM, Larson E, Chen AB. Clinical utility of 4D FDG-PET/CT scans in radiation treatment planning. Int J Radiat Oncol Biol Phys. 2012; 82:e99–105. [PubMed: 21377285]

Aristophanous M, Rottmann J, Park SJ, Nishioka S, Shirato H, Berbeco RI. Image-guided adaptive gating of lung cancer radiotherapy: a computer simulation study. Physics in medicine and biology. 2010; 55:4321–33. [PubMed: 20647609]

Aristophanous M, Yap JT, Killoran JH, Chen AB, Berbeco RI. Four-dimensional positron emission tomography: implications for dose painting of high-uptake regions. Int J Radiat Oncol Biol Phys. 2011; 80:900–8. [PubMed: 20950956]

Avril NE, Weber WA. Monitoring response to treatment in patients utilizing PET. Radiol Clin North Am. 2005; 43:189–204. [PubMed: 15693656]

Bentzen SM. Theragnostic imaging for radiation oncology: dose-painting by numbers. The lancet oncology. 2005; 6:112–7. [PubMed: 15683820]

Berbeco RI, Nishioka S, Shirato H, Chen GT, Jiang SB. Residual motion of lung tumours in gated radiotherapy with external respiratory surrogates. Physics in medicine and biology. 2005; 50:3655–67. [PubMed: 16077219]

Bettinardi V, Picchio M, Di Muzio N, Gianolli L, Gilardi MC, Messa C. Detection and compensation of organ/lesion motion using 4D-PET/CT respiratory gated acquisition techniques. Radiotherapy and oncology: journal of the European Society for Therapeutic Radiology and Oncology. 2010a; 96:311–6. [PubMed: 20708809]

Bettinardi V, Picchio M, Di Muzio N, Gianolli L, Messa C, Gilardi MC. PET/CT for radiotherapy: image acquisition and data processing. Q J Nucl Med Mol Imaging. 2010b; 54:455–75. [PubMed: 20927014]

Bettinardi V, Picchio M, Di Muzio N, Gilardi MC. Motion management in positron emission tomography/computed tomography for radiation treatment planning. Seminars in nuclear medicine. 2012; 42:289–307. [PubMed: 22840595]

Boellaard R. Standards for PET image acquisition and quantitative data analysis. Journal of nuclear medicine: official publication, Society of Nuclear Medicine. 2009; 50(Suppl 1):11S–20S.

Bortfeld T, Jiang SB, Rietzel E. Effects of motion on the total dose distribution. Seminars in radiation oncology. 2004; 14:41–51. [PubMed: 14752732]

Bowen SR, Flynn RT, Bentzen SM, Jeraj R. On the sensitivity of IMRT dose optimization to the mathematical form of a biological imaging-based prescription function. Phys Med Biol. 2009; 54:1483–501. [PubMed: 19218733]

Bowen SR, Nyflot MJ, Gensheimer M, Hendrickson KRG, Kinahan PE, Sandison GA, Patel SA. Challenges and opportunities in patient-specific, motion-managed, and PET/CT-guided radiation therapy of lung cancer: review and perspective. Clin Trans Med. 2012

Bradshaw TJ, Bowen SR, Jallow N, Forrest LJ, Jeraj R. Intratumor correlations of FDG, FLT, and Cu-ATSM PET in canine sarcoma and carcinoma tumors: implications for dose painting. J Nucl Med. 2013 in press.

Caldwell CB, Mah K, Ung YC, Danjoux CE, Balogh JM, Ganguli SN, Ehrlich LE. Observer variation in contouring gross tumor volume in patients with poorly defined non-small-cell lung tumors on CT: the impact of 18FDG-hybrid PET fusion. Int J Radiat Oncol Biol Phys. 2001; 51:923–31. [PubMed: 11704312]

Cheebsumon P, Boellaard R, de Ruysscher D, van Elmpt W, van Baardwijk A, Yaqub M, Hoekstra OS, Comans EF, Lammertsma AA, van Velden FH. Assessment of tumour size in PET/CT lung cancer studies: PET- and CT-based methods compared to pathology. EJNMMI research. 2012; 2:56. [PubMed: 23034289]

Choi B, Deasy JO. The generalized equivalent uniform dose function as a basis for intensity-modulated treatment planning. Physics in medicine and biology. 2002; 47:3579–89. [PubMed: 12433121]

Court LE, Seco J, Lu XQ, Ebe K, Mayo C, Ionascu D, Winey B, Giakoumakis N, Aristophanous M, Berbeco R, Rottman J, Bogdanov M, Schofield D, Lingos T. Use of a realistic breathing lung

phantom to evaluate dose delivery errors. Medical physics. 2010; 37:5850–7. [PubMed: 21158297]

De Ruysscher D, Nestle U, Jeraj R, Macmanus M. PET scans in radiotherapy planning of lung cancer. Lung Cancer. 2012; 75:141–5. [PubMed: 21920625]

Duan J, Shen S, Fiveash JB, Popple RA, Brezovich IA. Dosimetric and radiobiological impact of dose fractionation on respiratory motion induced IMRT delivery errors: a volumetric dose measurement study. Medical physics. 2006; 33:1380–7. [PubMed: 16752574]

Ezzell GA, Galvin JM, Low D, Palta JR, Rosen I, Sharpe MB, Xia P, Xiao Y, Xing L, Yu CX. Guidance document on delivery, treatment planning, and clinical implementation of IMRT: report of the IMRT Subcommittee of the AAPM Radiation Therapy Committee. Medical physics. 2003; 30:2089–115. [PubMed: 12945975]

Falk M, Larsson T, Keall P, Chul Cho B, Aznar M, Korreman S, Poulsen P, Munck Af, Rosenschold P. The dosimetric impact of inversely optimized arc radiotherapy plan modulation for real-time dynamic MLC tracking delivery. Medical physics. 2012; 39:1588–94. [PubMed: 22380391]

Flampouri S, Jiang SB, Sharp GC, Wolfgang J, Patel AA, Choi NC. Estimation of the delivered patient dose in lung IMRT treatment based on deformable registration of 4D-CT data and Monte Carlo simulations. Physics in medicine and biology. 2006; 51:2763–79. [PubMed: 16723765]

Ford EC, Herman J, Yorke E, Wahl RL. 18F-FDG PET/CT for image-guided and intensity-modulated radiotherapy. Journal of nuclear medicine: official publication, Society of Nuclear Medicine. 2009; 50:1655–65.

Ford EC, Kinahan PE, Hanlon L, Alessio A, Rajendran J, Schwartz DL, Phillips M. Tumor delineation using PET in head and neck cancers: threshold contouring and lesion volumes. Medical physics. 2006; 33:4280–8. [PubMed: 17153406]

Hatt M, Cheze le Rest C, Turzo A, Roux C, Visvikis D. A Fuzzy Locally Adaptive Bayesian Segmentation Approach for Volume Determination in PET. Medical Imaging, IEEE Transactions on. 2009; 28:881–93.

Herrmann, C.; Schilling, K. Improving Patient Comfort using Model Predictive Control in Robot-Assisted Radiotherapy. Proceedings of the IEEE International Conference on Robotics and Automation; Karlsruhe, Germany. 2013. p. 5426-32.

Imamura Y, Azuma K, Kurata S, Hattori S, Sasada T, Kinoshita T, Okamoto M, Kawayama T, Kaida H, Ishibashi M, Aizawa H. Prognostic value of SUVmax measurements obtained by FDG-PET in patients with non-small cell lung cancer receiving chemotherapy. Lung Cancer. 2011; 71:49–54. [PubMed: 20430470]

Juweid ME, Cheson BD. Positron-emission tomography and assessment of cancer therapy. The New England journal of medicine. 2006; 354:496–507. [PubMed: 16452561]

Keall PJ, Colvill E, O'Brien R, Ng JA, Poulsen PR, Eade T, Kneebone A, Booth JT. The first clinical implementation of electromagnetic transponder-guided MLC tracking. Medical physics. 2014; 41:020702. [PubMed: 24506591]

Keall PJ, Mageras GS, Balter JM, Emery RS, Forster KM, Jiang SB, Kapatoes JM, Low DA, Murphy MJ, Murray BR, Ramsey CR, Van Herk MB, Vedam SS, Wong JW, Yorke E. The management of respiratory motion in radiation oncology report of AAPM Task Group 76. Medical physics. 2006; 33:3874–900. [PubMed: 17089851]

Killoran JH, Gerbaudo VH, Mamede M, Ionascu D, Park SJ, Berbeco R. Motion artifacts occurring at the lung/diaphragm interface using 4D CT attenuation correction of 4D PET scans. Journal of applied clinical medical physics/American College of Medical Physics. 2011; 12:3502. [PubMed: 22089005]

Kissick MW, Mo X, McCall KC, Schubert LK, Westerly DC, Mackie TR. A phantom model demonstration of tomotherapy dose painting delivery, including managed respiratory motion without motion management. Physics in medicine and biology. 2010; 55:2983–95. [PubMed: 20436233]

Li G, Citrin D, Camphausen K, Mueller B, Burman C, Mychalczak B, Miller RW, Song Y. Advances in 4D medical imaging and 4D radiation therapy. Technology in cancer research & treatment. 2008; 7:67–81. [PubMed: 18198927]

Ling CC, Humm J, Larson S, Amols H, Fuks Z, Leibel S, Koutcher JA. Towards multidimensional radiotherapy (MD-CRT): biological imaging and biological conformality. Int J Radiat Oncol Biol Phys. 2000; 47:551–60. [PubMed: 10837935]

Liu C, Alessio A, Pierce L, Thielemans K, Wollenweber S, Ganin A, Kinahan P. Quiescent period respiratory gating for PET/CT. Medical physics. 2010; 37:5037–43. [PubMed: 20964223]

Liu C, Alessio AM, Kinahan PE. Respiratory motion correction for quantitative PET/CT using all detected events with internal-external motion correlation. Medical physics. 2011; 38:2715–23. [PubMed: 21776808]

Liu C, Pierce LA 2nd, Alessio AM, Kinahan PE. The impact of respiratory motion on tumor quantification and delineation in static PET/CT imaging. Physics in medicine and biology. 2009; 54:7345–62. [PubMed: 19926910]

Low DA, Dempsey JF. Evaluation of the gamma dose distribution comparison method. Medical physics. 2003; 30:2455–64. [PubMed: 14528967]

Mac Manus MP, Hicks RJ, Matthews JP, McKenzie A, Rischin D, Salminen EK, Ball DL. Positron emission tomography is superior to computed tomography scanning for response-assessment after radical radiotherapy or chemoradiotherapy in patients with non-small-cell lung cancer. Journal of clinical oncology: official journal of the American Society of Clinical Oncology. 2003; 21:1285–92. [PubMed: 12663716]

Menten MJ, Guckenberger M, Herrmann C, Krauss A, Nill S, Oelfke U, Wilbert J. Comparison of a multileaf collimator tracking system and a robotic treatment couch tracking system for organ motion compensation during radiotherapy. Medical physics. 2012; 39:7032–41. [PubMed: 23127094]

Nehmeh SA, Erdi YE, Pan T, Yorke E, Mageras GS, Rosenzweig KE, Schoder H, Mostafavi H, Squire O, Pevsner A, Larson SM, Humm JL. Quantitation of respiratory motion during 4D-PET/CT acquisition. Medical physics. 2004; 31:1333–8. [PubMed: 15259636]

Nehmeh SA, Haj-Ali AA, Qing C, Stearns C, Kalaigian H, Kohlmyer S, Schoder H, Ho AY, Larson SM, Humm JL. A novel respiratory tracking system for smart-gated PET acquisition. Medical physics. 2011; 38:531–8. [PubMed: 21361220]

Nestle U, Kremp S, Grosu AL. Practical integration of [(18)F]-FDG-PET and PET-CT in the planning of radiotherapy for non-small cell lung cancer (NSCLC): The technical basis, ICRU-target volumes, problems, perspectives. Radiotherapy and Oncology. 2006; 81:209–25. [PubMed: 17064802]

Nestle U, Kremp S, Schaefer-Schuler A, Sebastian-Welsch C, Hellwig D, Rube C, Kirsch CM. Comparison of different methods for delineation of 18F-FDG PET-positive tissue for target volume definition in radiotherapy of patients with non-Small cell lung cancer. Journal of nuclear medicine: official publication, Society of Nuclear Medicine. 2005; 46:1342–8.

Nyflot MJ, Harari PM, Yip S, Perlman SB, Jeraj R. Correlation of PET images of metabolism, proliferation and hypoxia to characterize tumor phenotype in patients with cancer of the oropharynx. Radiotherapy and oncology: journal of the European Society for Therapeutic Radiology and Oncology. 2012; 105:36–40. [PubMed: 23068711]

Schleyer PJ, O'Doherty MJ, Barrington SF, Marsden PK. Retrospective data-driven respiratory gating for PET/CT. Physics in medicine and biology. 2009; 54:1935–50. [PubMed: 19265207]

Schleyer PJ, O'Doherty MJ, Marsden PK. Extension of a data-driven gating technique to 3D, whole body PET studies. Physics in medicine and biology. 2011; 56:3953–65. [PubMed: 21666288]

Senan S, De Ruysscher D. Critical review of PET-CT for radiotherapy planning in lung cancer. Critical reviews in oncology/hematology. 2005; 56:345–51. [PubMed: 15990331]

Shah C, Kestin LL, Hope AJ, Bissonnette JP, Guckenberger M, Xiao Y, Sonke JJ, Belderbos J, Yan D, Grills IS. Required target margins for image-guided lung SBRT: Assessment of target position intrafraction and correction residuals. Practical radiation oncology. 2013; 3:67–73. [PubMed: 24674265]

Teras M, Tolvanen T, Johansson JJ, Williams JJ, Knuuti J. Performance of the new generation of whole-body PET/CT scanners: Discovery STE and Discovery VCT. European journal of nuclear medicine and molecular imaging. 2007; 34:1683–92. [PubMed: 17661031]

Tylski P, Stute S, Grotus N, Doyeux K, Hapdey S, Gardin I, Vanderlinden B, Buvat I. Comparative assessment of methods for estimating tumor volume and standardized uptake value in (18)F-FDG PET. Journal of nuclear medicine: official publication, Society of Nuclear Medicine. 2010; 51:268–76.

van Elmpt W, Hamill J, Jones J, De Ruysscher D, Lambin P, Ollers M. Optimal gating compared to 3D and 4D PET reconstruction for characterization of lung tumours. European journal of nuclear medicine and molecular imaging. 2011; 38:843–55. [PubMed: 21222120]

van Elmpt W, Ollers M, Dingemans AM, Lambin P, De Ruysscher D. Response assessment using 18F-FDG PET early in the course of radiotherapy correlates with survival in advanced-stage non-small cell lung cancer. Journal of nuclear medicine: official publication, Society of Nuclear Medicine. 2012; 53:1514–20.

Vansteenkiste JF, Stroobants SG, De Leyn PR, Dupont PJ, Bogaert J, Maes A, Deneffe GJ, Nackaerts KL, Verschakelen JA, Lerut TE, Mortelmans LA, Demedts MG. Lymph node staging in non-small-cell lung cancer with FDG-PET scan: a prospective study on 690 lymph node stations from 68 patients. Journal of clinical oncology: official journal of the American Society of Clinical Oncology. 1998; 16:2142–9. [PubMed: 9626214]

Webb S. Motion effects in (intensity modulated) radiation therapy: a review. Physics in medicine and biology. 2006a; 51:R403–25. [PubMed: 16790915]

Webb S. Quantification of the fluence error in the motion-compensated dynamic MLC (DMLC) technique for delivering intensity-modulated radiotherapy (IMRT). Physics in medicine and biology. 2006b; 51:L17–21. [PubMed: 16552094]

Weber WA, Grosu AL, Czernin J. Technology Insight: advances in molecular imaging and an appraisal of PET/CT scanning. Nature clinical practice. Oncology. 2008; 5:160–70.

Wilbert J, Baier K, Hermann C, Flentje M, Guckenberger M. Accuracy of real-time couch tracking during 3-dimensional conformal radiation therapy, intensity modulated radiation therapy, and volumetric modulated arc therapy for prostate cancer. Int J Radiat Oncol Biol Phys. 2013; 85:237–42. [PubMed: 22541958]

Wilbert J, Meyer J, Baier K, Guckenberger M, Herrmann C, Hess R, Janka C, Ma L, Mersebach T, Richter A, Roth M, Schilling K, Flentje M. Tumor tracking and motion compensation with an adaptive tumor tracking system (ATTS): system description and prototype testing. Medical physics. 2008; 35:3911–21. [PubMed: 18841842]

Wu Q, Djajaputra D, Liu HH, Dong L, Mohan R, Wu Y. Dose sculpting with generalized equivalent uniform dose. Medical physics. 2005; 32:1387–96. [PubMed: 15984690]

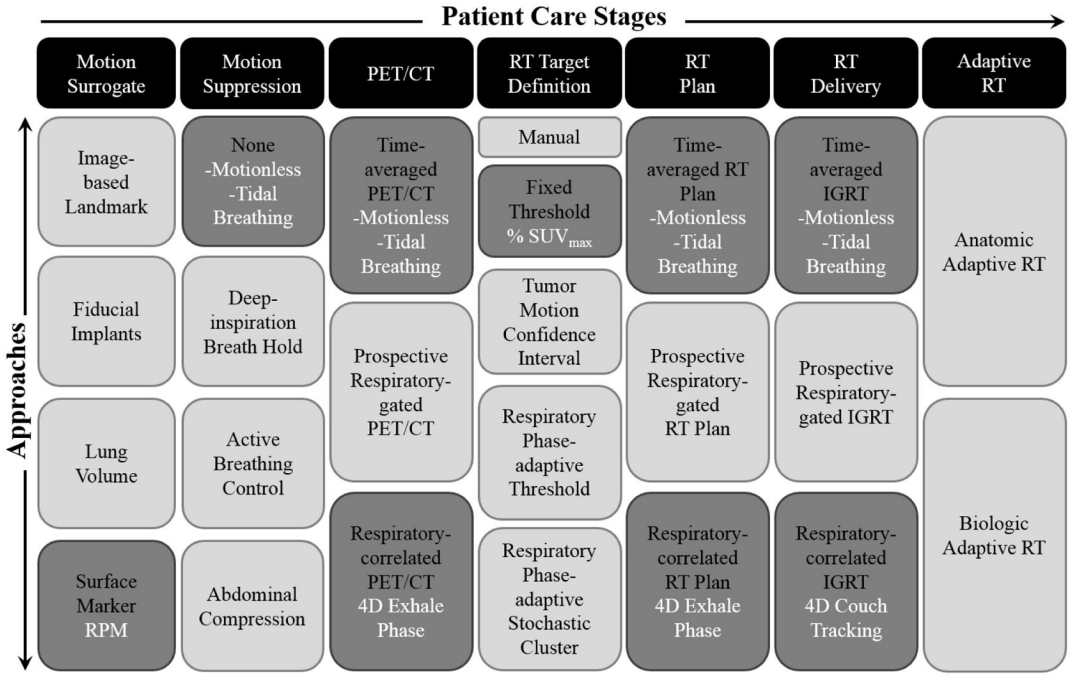

Figure 1. End-to-end characterization of respiratory motion-induced errors in PET/CT-guided radiotherapy

Relative to ground truth (motionless) measurements, errors due to respiratory motion blurring (tidal motion) and motion compensation (4D imaging and therapy) are estimated. Errors propagate along a chain of patient care stages that span motion surrogate, motion suppression, PET/CT acquisition and reconstruction, radiotherapy target definition, treatment planning, treatment delivery, and adaptive radiotherapy. Approaches investigated in this study are highlighted (dark grey fill) and list the conditions tested (white text).

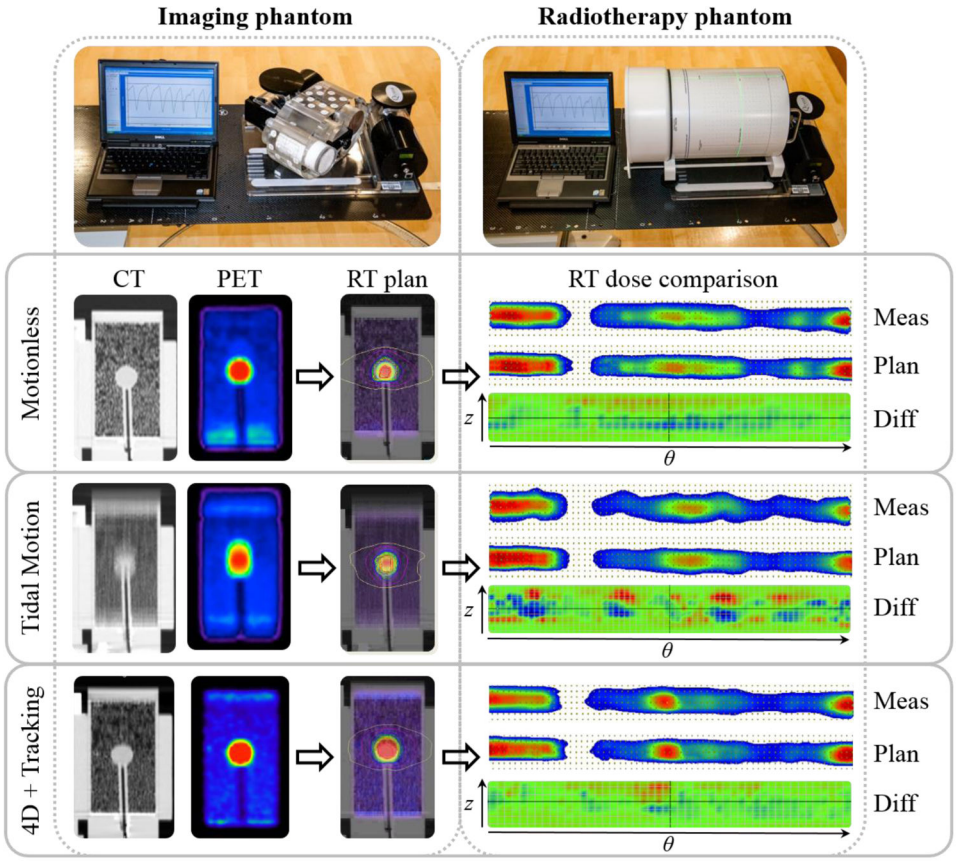

Figure 2. Error estimation in PET/CT-guided radiotherapy of lung cancer using dynamic motion imaging and radiotherapy phantoms

An example patient respiratory motion pattern (Table 1: pattern 1) drives the lung insert and lesion (2.2 cm diameter, 10:1 contrast) in an imaging phantom, which can generate treatment plans that can be delivered under the same or different motion patterns to the radiotherapy phantom. Differences in delivered dose are scaled from −10 cGy (blue) to +10 cGy (red).

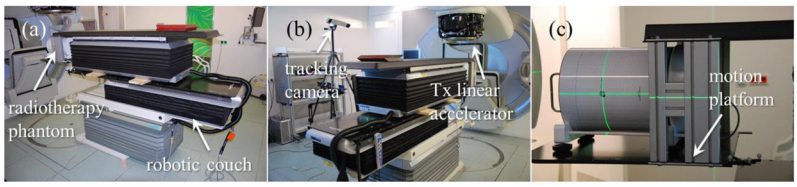

Figure 3. Robotic couch motion compensation with infrared camera tracking for 4D radiotherapy delivery

(a) Two HexaPOD tables with 6 degrees of freedom were used to independently move and track the ArcCHECK diode detector array. (b) The Polaris infrared camera recorded the relative difference in the position of reflective markers placed on moving and motion-compensating platforms. (c) The ArcCHECK was aligned to the machine isocentre prior to static delivery, motion-blurred delivery, and motion-tracked delivery.

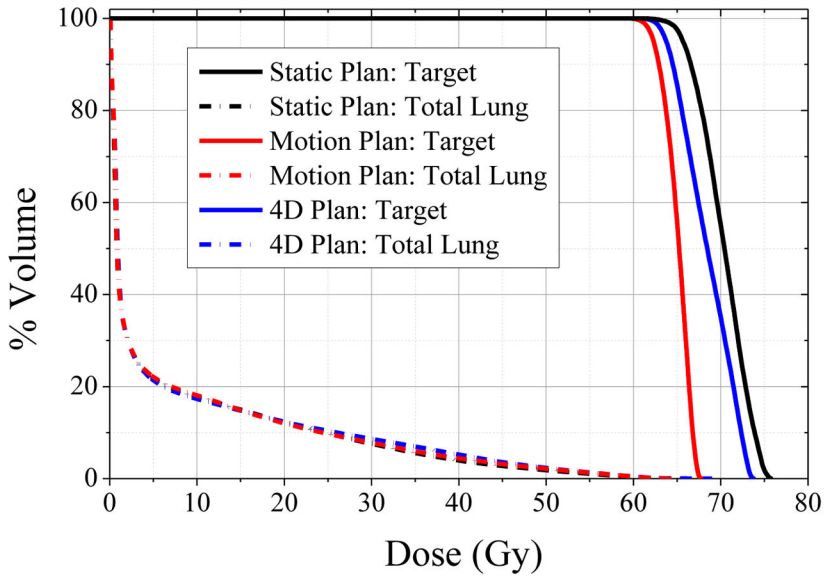

Figure 4. Dose volume histograms of the reference static PET-based plan (black lines), motion-blurred PET-based plan (red lines), and motion-compensated PET-based plan (blue lines)

For similar total lung DVH, maximum and equivalent uniform doses in the PET-based targets vary considerably. Note only the set of planned doses from the respiratory pattern with median error magnitude is shown for clarity (Table 1: pattern 1).

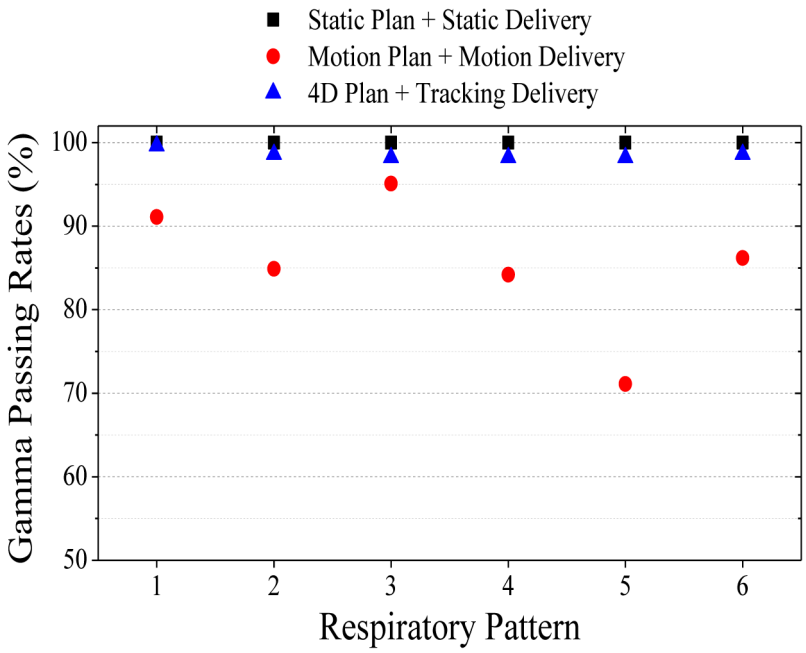

Figure 5. Respiratory-motion induced errors in radiotherapy delivery accuracy

Gamma passing rates (2%-2mm criteria) were recorded for a reference static PET-based plan delivered under no motion (black squares). Gamma values were also calculated for six patient respiratory patterns with motion trajectories that moved the ArcCHECK phantom during delivery of a motion-blurred PET-based plan (red circles) and a motion-compensated PET-based plan with couch tracking (blue triangles).

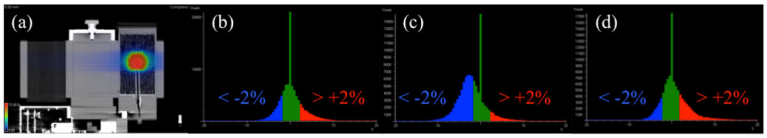

Figure 6. Errors in delivered dose reconstructed on PET/CT imaging phantom

(a) Measured dose under motion-compensated delivery reconstructed on end-expiration respiratory-gated cine CT. The dose difference histograms between measured and planned distributions with colour bar difference < −2% (blue), ±2% (green), > +2% (red) error for (b) static, (c) motion-blurred, and (d) motion-compensated delivery. Note only the set of delivered doses distributions from the respiratory pattern with median error magnitude is shown for clarity (Table 1: pattern 1).

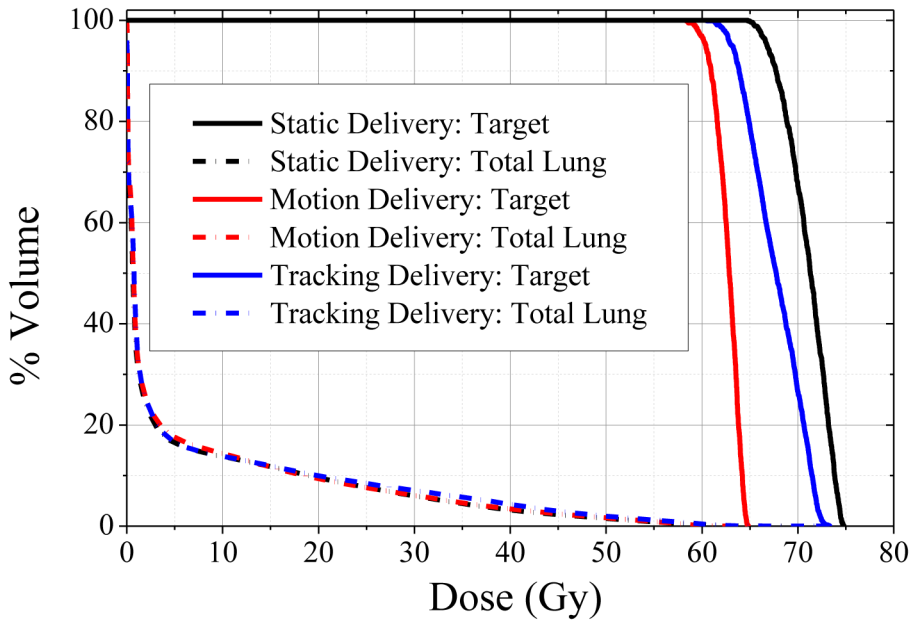

Figure 7. Dose volume histograms under reference static delivery conditions (black lines), motion-blurred delivery (red lines), and motion-compensated delivery (blue lines)

Differences in target dose distribution have increased between the various delivery conditions, particularly for the delivery under motion, with respect to the planned dose differences of Figure 4. Note only the set of delivered doses from the patient respiratory pattern with median error magnitude is shown for clarity (Table 1: pattern 1).

Table 1

Patient-specific respiratory patterns

Mean ± standard deviation in amplitude and period, as well as deviation in displacement and velocity is reported for 6 patient respiratory waveforms. The trajectories were applied to the imaging and radiotherapy phantoms in the superior-inferior dimension (1D).

Patient Respiratory Pattern	Amplitude (cm)	Period (s)	Displacement Deviation (cm)	Velocity Deviation (cm/s)
1	0.8 ± 0.2	4.0 ± 1.3	0.3	0.5
2	1.1 ± 0.1	3.8 ± 0.3	0.4	0.6
3	0.6 ± 0.1	3.5 ± 0.4	0.2	0.3
4	1.2 ± 0.1	3.6 ± 0.3	0.4	0.7
5	1.2 ± 0.2	6.2 ± 1.5	0.5	0.4
6	1.0 ± 0.8	3.3 ± 0.6	0.3	0.6

Table 2

Respiratory-motion induced errors estimated during PET/CT imaging, radiotherapy (RT) planning, and RT delivery

Median errors (interquartile ranges) in tumour-to-background maximum ratios, fixed threshold volumes, planned and measured maximum target doses, and delivery accuracy rates were recorded. Aggregate error was both calculated under assumption of independent error component summation in quadrature as well as direct estimate from measurement.

Process	Parameter	Motionless Ground Truth	Tidal Motion Error	Motion Compensation Residual Error
PET/CT Imaging	T/B_{max}	11.2	−20% (12%)	−8% (5%)
	SUV_{max} Fixed Threshold Volume	5.6 cm^3	+15% (9%)	+7% (4%)
RT Planning	Plan Max Target Dose	76 Gy	−10% (6%)	−3% (2%)
	Equivalent Uniform Target Plan Dose	70 Gy	−7% (4%)	−2% (1%)
RT Delivery	Measured Max Target Dose	75 Gy	−9% (5%)	−1% (1%)
	Accuracy 2% Diff + 2mm DTA	100%	−15% (9%)	−1% (1%)
Aggregate Error	Calculated	-	24% (14%)	9% (5%)
	Measured	-	17% (9%)	4% (2%)